Advanced Steel Construction – Vol. 19 No. 2 (2023) 150–156
DOI:10.18057/IJASC.2023.19.2.7

EXPERIMENTAL STUDY ON INTERACTION OF DISTORTIONAL AND GLOBAL BUCKLING OF STAINLESS STEEL LIPPED CHANNEL COLUMNS

Mei-Jing Liu [1], Jun-Feng Liu [2], Mei-He Chen [3, *], Guang-Ming Yu [4], Sheng-Gang Fan [5] and Cheng-Long Wan [3]

[1] *Department of Civil Engineering, Southeast University Chengxian College, Nanjing, China*
[2] *Three Gorges Renewables Yangjiang Power Co.,Ltd.,Yangjiang,Guangdong, China*
[3] *China Academy of Building Research, Beijing, China*
[4] *Institute of Science and Technology, China Three Gorges Corporation, Beijing, China*
[5] *Key Laboratory of Concrete and Prestressed Concrete Structures of Ministry of Education, School of Civil Engineering, Southeast University, Jiulonghu Campus, Nanjing, China*
** (Corresponding author: E-mail: mhechen@163.com)*

ABSTRACT

This paper presents an experimental program to investigate distortional and global interaction buckling of stainless steel lipped channel columns in compression. Appropriate cross-sections and lengths were chosen so as to observe distortional-overall interaction buckling. In total, 21 buckling tests were conducted. After a brief introduction to the choice of column specimen geometries, key experimental results have been presented and discussed. The tests aim to study and observe the effect of distortional-global interactive buckling, study member under pin-ended boundary conditions, and provide benchmarks for design. Column tests were carried out with 13 position transducers monitoring displacements at key locations. A 3-D laser scanner was used to measure the imperfection shapes and magnitudes of the columns before testing. Material tests have been performed to determine the mechanical properties of stainless steel. Distortional–global interactive buckling of all columns is shown to be a failure mode. The experimental results are also used to evaluate the Australian Standard AS/NZS, North American Specification AISI, as well as formulation proposed by Becque and Rasmussen's predictions, indicated that the Direct Strength Method (DSM) as described in AISI and AS/NZS for members undergoing distortional-overall interaction buckling are unconservative. Becque and Rasmussen's curve is much closer to the test points than DSM in AISI and AS/NZS.

ARTICLE HISTORY

Received: 8 August 2022
Revised: 16 December 2022
Accepted: 29 December 2022

KEYWORDS

Stainless steel;
Buckling mode interaction;
Lipped channel column;
Direct strength method;
Axial compression test

1. Introduction

Compared to carbon steel, stainless steel has attractive features in appearance, corrosion resistance, and fire resistance rating [1-3]. Stainless steel is also 100% recyclable and retains its good mechanical and physical properties after recycling [3]. Stainless steel is widely used in all walks of life and has attracted much attention. In addition, the boom in stainless steel production with continuous improvement in processing methods offers the possibility of more use in building structures.

As architects, designers and researchers are becoming aware of the good properties of stainless steel, many research projects have been conducted, including material properties [4-7], lipped channel columns [8-19], channel columns [20-23], I-section columns [24-29] and hollow section [30-35]. These research results have led to significant advances in design and application in the construction industry. However, tests performed on columns have mainly investigated failure by local, distortional, and global buckling. Currently, There needs to be more investigations on distortional-overall interaction buckling.

This paper aims to present an experimental program to study the distortional-overall interaction buckling in S30408 stainless steel lipped channels. Material tensile tests were first performed to investigate the mechanical properties of stainless steel. Then the imperfections were measured to obtain the imperfection distribution patterns and the maximum imperfection values of local, distortional and overall buckling. Axial compression tests on 21 columns were conducted to investigate the buckling damage characteristics of stainless steel columns. The test specimens are axially compressed while the columns are designed to undergo distortional-overall interaction buckling. The focus in this experimental program is to study the distortional-overall interaction buckling.

2. Material properties

Material property studies on stainless steel alloy materials are essential for designing appropriate sections and evaluating the strengths of the designed sections. Material tests have been carried out to study the mechanical behavior of stainless steel. Specimens were extracted from 1.5mm and 1.8mm columns using a laser cutter, as shown in Fig. 1.

The specimens were tested following the code of metallic materials-tensile testing [36]. The fractures of the tensile specimens after stretching were shown in Fig. 2, indicating that the specimens have a small necking range and a smooth fracture. The coupons were elongated after stretching, with good elongation of up to nearly 60%.

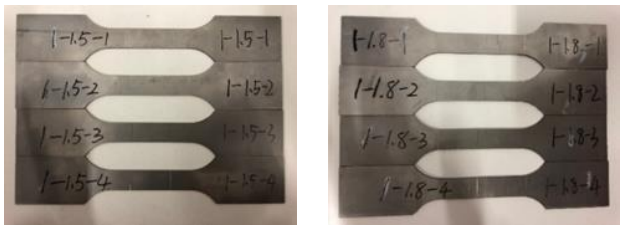

(a) 1.5mm coupons (b) 1.8mm coupons

Fig. 1 Tensile specimen

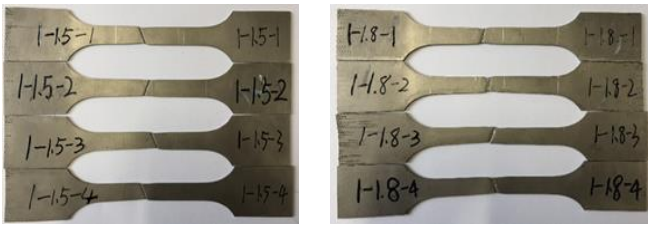

(a) 1.5mm coupons (b) 1.8mm coupons

Fig. 2 After tensile failure

Tensile results are listed in Table 1. In the table, E_0 is the material Young's modulus; $\sigma_{0.01}$ and $\sigma_{1.0}$ are the stresses corresponding to 0.01% and 1.0% residual deformation, respectively; $\sigma_{0.2}$ is the material 0.2% proof stress; σ_u is the peak material load; $\varepsilon_{t0.01}$, $\varepsilon_{t0.2}$, $\varepsilon_{t1.0}$ represent the strain corresponding to $\sigma_{0.01}$, $\sigma_{0.2}$, $\sigma_{1.0}$; ε_f is the elongation. The measured stress-strain relationships are shown in Fig. 3, indicating that stainless steel has a strong nonlinearity.

Table 1
Tensile properties

Specimen code	E_0 (MPa)	$\sigma_{0.01}$ (MPa)	$\sigma_{0.2}$ (MPa)	$\sigma_{1.0}$ (MPa)	σ_u (MPa)	$\varepsilon_{t0.01}$ (%)	$\varepsilon_{t0.2}$ (%)	$\varepsilon_{t1.0}$ (%)	ε_f (%)
F-1.5-1	192653	206.3	269.0	313.4	766.7	0.117	0.340	1.163	58.00
F-1.5-2	202049	242.2	272.3	309.9	767.3	0.130	0.335	1.153	63.00
F-1.5-3	215321	240.4	273.4	313.3	767.5	0.122	0.327	1.146	66.00
F-1.5-4	202148	230.3	270.4	312.9	763.2	0.124	0.334	1.155	64.00
Average	203042	229.8	271.3	312.4	766.2	0.123	0.334	1.154	62.75
F-1.8-1	206867	217.4	287.4	333.2	756.7	0.115	0.339	1.161	60.00
F-1.8-2	193045	220.1	281.5	325.4	758.0	0.124	0.346	1.169	58.00
F-1.8-3	202695	235.7	286.1	330.3	757.3	0.126	0.341	1.163	62.00
F-1.8-4	193299	245.9	285.4	328.4	770.0	0.137	0.348	1.170	60.00
Average	198977	229.8	285.1	329.3	760.5	0.126	0.344	1.166	60.00

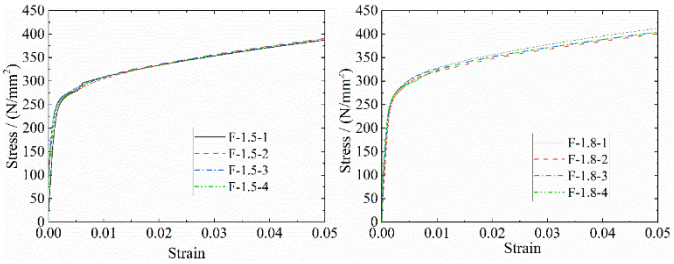

(a) 1.5mm (b) 1.8mm

Fig. 3 Measured Stress–strain relationships

3. Experimental investigation

3.1. Test setup

To investigate the distortional and overall interaction buckling of the channels. A total of 21 specimens hinged at both ends were conducted. The columns can rotate around the weak axis during the test. A test loading instrument (WDW-100) with high accuracy was used to conduct the test, as shown in Fig. 4. The single knife-edge bearing was used in the experiment, and the supports were lubricated, as shown in Fig. 5 (b). The complete experimental setup is illustrated in Fig. 5 (a). Four M16 bolts connected the support and the channel, and the end plates were connected with the support bottom plate as a whole to ensure that there was no relative sliding between the test column and the loading plate. A straight ruler was used to measure distortional buckling during the test, as shown in Fig. 5.

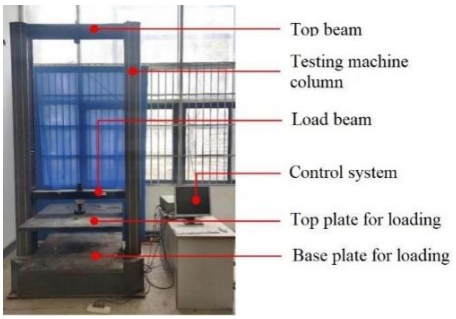

Fig. 4 Test loading instrument (WDW-100)

(a) Set-up (b) Specimen boundary conditions

Fig. 5 Test set-up

To study the cross-sectional stress variation with load at the middle of the column height during loading, 20 strain gauges were placed on each column, and the strain gauges were located on the inside and outside of the flanges, lips, and web. The numbers in parentheses in Fig. 6 are the numbers of the strain gauges inside the channels. The strain gauge data was obtained by the dynamic strain data acquisition instrument TDS-630, as shown in Fig. 7.

To obtain the axial displacements and lateral displacements of the channels, as well as the rotation angles of the support at both ends of the column, 13 LVDTs were installed on the specimens. The axial shortenings and the rotation angles of the columns can be obtained based on the results of LVDTs 6, 7, 8, 9, 10, 11, 12 and 13, and the lateral displacements can be calculated from the results of LVDTs 1, 2, 3, 4 and 5, as shown in Fig. 8.

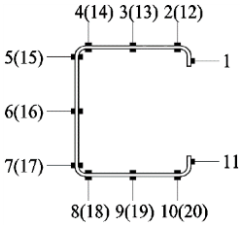

Fig. 6 Location of strain gauges **Fig. 7** TDS-630 Dynamic strain collector

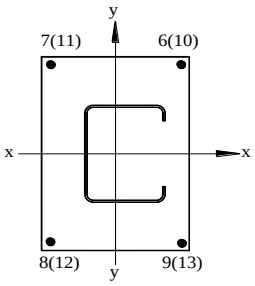

(a) Axial LVDTs at end plate

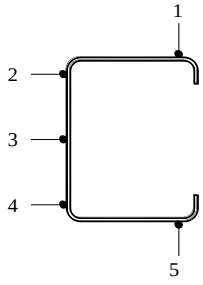

(b) Lateral LVDTs at column mid-height

Fig. 8 Location of LVDTs

Plates 20mm thick were welded at each end of the column to facilitate test loading and uniform force transfer. The dimensions of the plates are 240mm in

length and 160mm in width. All the finished test columns are shown in Fig. 9.

Fig. 9 Stainless steel column specimens

3.2. Specimen selection

The first step of the test is to design specimen dimensions, i.e., the cross-sectional sizes and the specimen lengths. The specimens were designed according to the CUFSM [37] buckling analysis results. The stainless steel columns were designed so that they have an interaction of distortional and global buckling modes. Fig. 10 shows a typical signature curve with two minimal value points: the local and distortional buckling half-wavelengths, respectively. The local buckling half-wavelength is smaller than the distortional buckling half-wavelength.

The column length is a key factor in determining what kind of buckling occurs in the column. First, the column should meet the requirements of $1.2P_{crd} < P_{crl}$ and $1.2P_{crg} < P_{crl}$, where P_{crd}, P_{crl} and P_{crg} are distortional, local and global buckling strength, respectively. Then $0.9P_{crd} < P_{crg} < 1.1P_{crd}$ should be satisfied. The specimen length should be greater than the distortional buckling half-wavelength. The global buckling of the specimen should be avoided, which means that the column length should be moderate.

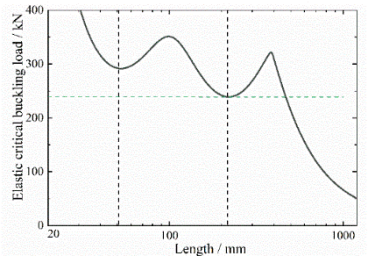

Fig. 10 Stainless steel column specimens

Table 2 lists the measured values of the columns, and the symbols are illustrated in Fig. 11. The column lengths here is the length of the stainless steel lipped channels, excluding the thickness of the end plates at both ends of the specimen.

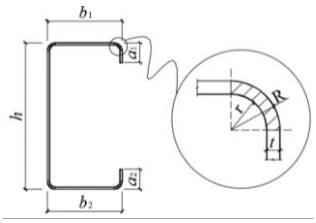

Fig. 11 Symbol definitions

3.3. Imperfection measurements

To improve the measurement accuracy, A 3-D laser scanner was used to measure the imperfection shapes and magnitudes of the columns prior to testing, as shown in Fig. 12 (a). The laser has an accuracy of 0.0001mm. The measurement process is as follows: firstly, mark points were attached to the test specimen, and then the 3-D laser scanner was used to scan the test column as a whole to obtain the data points, as shown in Fig. 12 (b).

Table 2
Measured dimensions (in mm)

Specimen code	Section code	h / mm	b_1 / mm	b_2 / mm	a_1 / mm	a_2 / mm	t / mm	Length / mm	r / mm
PP-1	C60×35×10×1.8	60.4	35.4	35.2	10.1	10.6	1.9	450.0	3.0
PP-2	C60×40×12×1.8	60.7	40.6	40.8	12.2	12.7	1.9	480.0	3.0
PP-3	C60×40×10×1.5	60.2	40.0	40.4	10.2	9.9	1.4	600.0	3.0
PP-4	C65×45×12×1.8	65.8	45.7	46.0	12.1	12.6	1.9	560.0	3.0
PP-5	C65×60×12×1.5	65.3	60.6	60.8	12.3	12.0	1.4	760.0	3.0
PP-6	C70×55×15×1.8	71.0	54.9	55.0	15.3	15.2	1.9	680.0	3.0
PP-7	C70×55×10×1.5	70.4	55.2	55.2	10.4	9.9	1.4	780.0	3.0
PP-8	C75×60×14×1.8	76.0	60.4	60.5	14.1	14.8	1.9	790.0	3.0
PP-9	C75×60×12×1.8	76.0	60.5	60.4	12.4	12.5	1.9	840.0	3.0
PP-10	C75×50×12×1.8	76.2	51.0	50.2	12.2	12.6	1.9	710.0	3.0
PP-11	C80×55×12×1.8	79.1	56.2	55.9	12.1	12.1	1.9	820.0	3.0
PP-12	C80×70×14×1.5	80.0	70.1	70.5	14.0	14.1	1.4	1000.0	3.0
PP-13	C80×65×12×1.5	80.2	65.1	65.1	12.1	12.2	1.4	1020.0	3.0
PP-14	C85×60×12×1.8	85.7	61.1	60.4	12.4	12.6	1.9	950.0	3.0
PP-15	C85×70×12×1.8	86.0	70.2	70.6	12.6	12.5	1.9	1050.0	3.0
PP-16	C85×70×15×1.8	85.0	70.8	70.1	15.6	15.8	1.9	1100.0	3.0
PP-17	C85×65×12×1.8	85.3	65.1	65.0	12.1	12.0	1.9	1080.0	3.0
PP-18-1	C88×60×12×1.8	88.2	60.7	60.4	12.4	12.7	1.9	960.0	3.0
PP-18-2	C88×60×12×1.8	88.5	60.9	60.3	12.4	13.0	1.9	960.0	3.0
PP-19-1	C96×68×12×1.8	96.6	68.5	69.0	12.3	11.9	1.9	1160.0	3.0
PP-19-2	C96×68×12×1.8	96.5	69.6	67.9	12.6	12.5	1.9	1160.0	3.0

Note: h is section height; b_1 and b_2 are upper and lower flange widths, separately; a_1 and a_2 are upper and lower lips widths, separately; t is thickness; l is column length; r is

Fig. 13 shows the imperfection distribution form of the PP-1 column. The imperfection distribution is not asymmetric and has a random nature. The imperfections were extracted along the lines in Fig. 14. Fig. 15 shows the measured imperfections of PP-1. Table 3 lists the maximum magnitude of

distortional, local and overall imperfections for the specimens. The overall initial imperfection amplitudes of the stainless steel columns are small, all less than one-thousandth of the column length, which can meet the requirements in the GB 50205-2001 [38]. The maximum imperfections amplitude of distortional and local buckling are 0.42mm and 0.40mm, respectively.

(a) 3-D laser scanner

(b) Measuring procedure

Fig. 12 Imperfection measurement

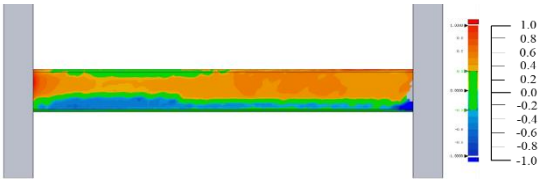

Fig. 13 Imperfection profile of PP-1

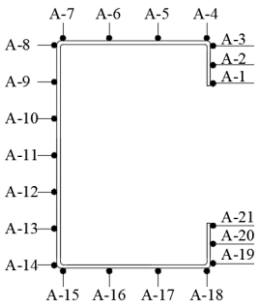

Fig. 14 Locations of the imperfection lines

Table 3
Maximum measured values of distortional, local and global buckling imperfections (in mm)

Specimen	Location	Local	Distortional	Global	Specimen	Location	Local	Distortional	Global
PP-1	Web	0.40	0.21	0.19	PP-11	Web	0.14	0.31	0.58
	Flange-up	0.32				Flange-up	0.26		
	Flange-down	0.29				Flange-down	0.11		
PP-2	Web	0.37	0.36	0.32	PP-12	Web	0.17	0.42	0.33
	Flange-up	0.13				Flange-up	0.11		
	Flange-down	0.36				Flange-down	0.24		
PP-3	Web	0.33	0.34	0.59	PP-13	Web	0.19	0.18	0.18
	Flange-up	0.19				Flange-up	0.25		
	Flange-down	0.19				Flange-down	0.29		
PP-4	Web	0.29	0.29	0.46	PP-14	Web	0.33	0.19	0.56
	Flange-up	0.29				Flange-up	0.40		
	Flange-down	0.21				Flange-down	0.29		
PP-5	Web	0.38	0.32	0.53	PP-15	Web	0.31	0.24	0.34
	Flange-up	0.33				Flange-up	0.17		
	Flange-down	0.39				Flange-down	0.31		
PP-6	Web	0.15	0.41	0.57	PP-16	Web	0.12	0.35	0.13
	Flange-up	0.29				Flange-up	0.18		
	Flange-down	0.31				Flange-down	0.19		
PP-7	Web	0.21	0.35	0.34	PP-17	Web	0.30	0.26	0.16
	Flange-up	0.37				Flange-up	0.23		
	Flange-down	0.32				Flange-down	0.28		
PP-8	Web	0.12	0.23	0.49	PP-18-1	Web	0.25	0.21	0.58
	Flange-up	0.16				Flange-up	0.33		
	Flange-down	0.15				Flange-down	0.34		
PP-9	Web	0.38	0.33	0.49	PP-18-2	Web	0.28	0.14	0.60
	Flange-up	0.24				Flange-up	0.23		
	Flange-down	0.35				Flange-down	0.21		
PP-10	Web	0.20	0.32	0.60	PP-19-1	Web	0.38	0.24	0.34
	Flange-up	0.38				Flange-up	0.26		
	Flange-down	0.16				Flange-down	0.34		

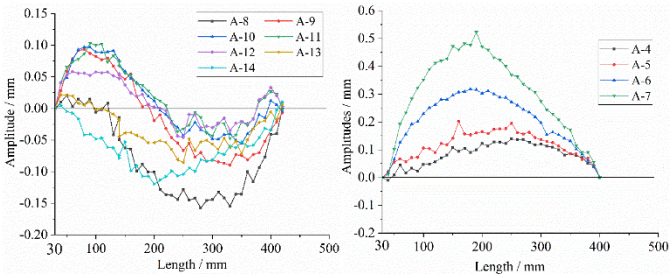

(a) A-8 ~ A-14 (b) A-4 ~ A-7

Fig. 15 Typical imperfection profile

4. Test results

4.1. Load-deformation curves

All experimental columns were expected to fail by distortional-overall interaction buckling. From the test observations, this hypothesis holds. Fig. 16 shows load–axial displacement relationships of the channels. The trends of the load-axial displacement relationships are basically the same. When the load is loaded, the axial displacement increases linearly with the increase of the load. As the load continues to increase, the stiffness of the specimen begins to decrease, and the load and displacement show a nonlinear relationship until the stiffness decreases to zero. The nonlinear part of the curve is relatively short, and the load soon reaches the peak load.

For PP-1 and PP-2, after the loads reach the peak loads, the load–axial displacements decrease slowly and no sudden damage occurs in the specimens. The reason why the specimens did not suffer sudden damage may be that the specimen lengths are relatively short and the boundary constraint plays a certain strengthening role. For other specimens, when the loads reach the peak loads, the load–axial displacement curves suddenly drop sharply, and the axial displacements suddenly increase. All specimens basically have no post-buckling strength.

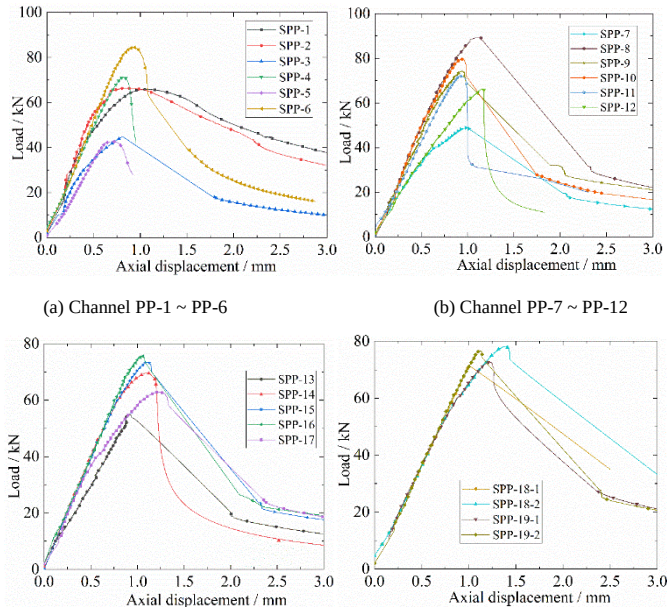

(a) Channel PP-1 ~ PP-6 (b) Channel PP-7 ~ PP-12

(c) Channel PP-1 ~ PP-6 (d) Channel PP-7 ~ PP-12

Fig. 16 Load vs. axial displacement curves

4.2. Load-rotation curves

During the experiment, the stainless steel columns were rotated around the weak axis of the section. According to the axial displacement values of the measuring points obtained by the axial LVDTs at end plates, the rotation angles can be calculated. Fig. 17 plots the load vs. the rotation of specimens PP-3, PP-6, PP-16, and PP-17. The diagrams in Fig. 17 show that the curves of both rotations of upper and lower supports are consistent, indicating that the upper and lower end plates have the same rotation angle, and the specimens were not twisted. This is consistent with the observed experimental phenomena.

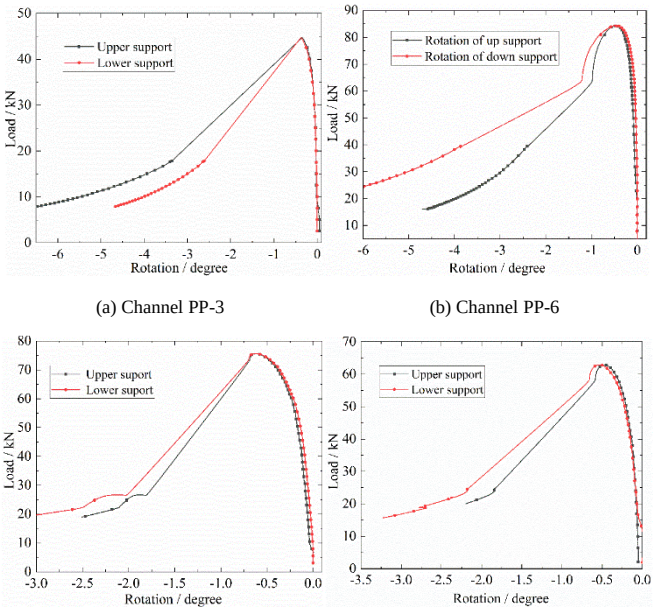

(a) Channel PP-3 (b) Channel PP-6

(c) Channel PP-16 (d) Channel PP-17

Fig. 17 Load vs. rotation curves

4.3. Load-lateral displacement relationships

The load-lateral displacement relationships of the PP-2, PP-6, PP-10, and PP-16 are shown in 18, indicating that the columns were not twisted, which is consistent with the conclusion identified in Fig. 17. Fig. 18 also shows that the lateral displacement of both LVDT 2 and 4 are earlier and larger than the lateral displacement of both LVDT 1 and 5, which indicates that the global buckling is earlier than distortional buckling.

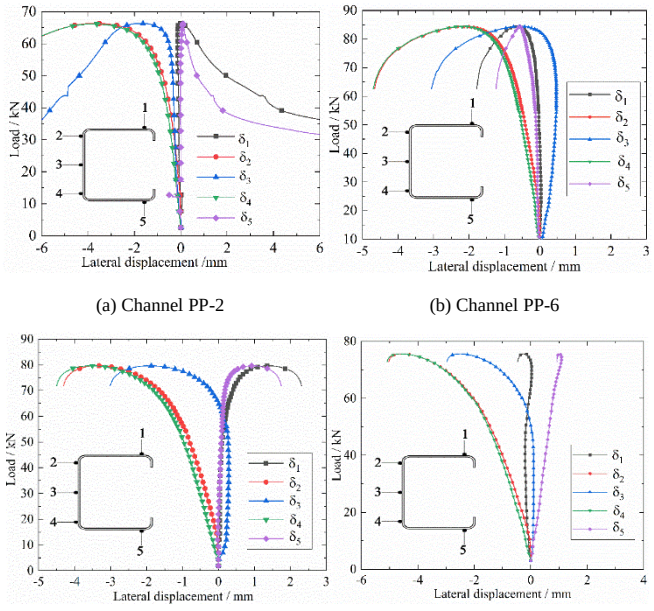

(a) Channel PP-2 (b) Channel PP-6

(c) Channel PP-10 (d) Channel PP-16

Fig. 18 Load vs. lateral displacement curves

4.4. Failure modes

All 21 columns were seen to show global buckling first, followed by eventual failure by distortional-global interaction buckling. No local buckling was visually seen in the designed channels. The peak strengths and buckling modes obtained from the test are detailed in Table 4. P_u is the ultimate capacity; D and G mean distortional and overall buckling, respectively; D+G means distortional-overall interactive buckling.

Observing the distortional buckling during the test is difficult, and the collected data can not reflect it in time. Moreover, distortional buckling has small post-buckling strength, and the specimen will reach the buckling damage soon after distortional buckling occurs. Therefore, to better observe the

distortional buckling, a ruler was used to measure the distance between the two lips, as shown in Fig. 19. If the distance between the two lips changes, the specimen can be judged to occur distortional buckling.

Fig. 14 Locations of the imperfection lines

Table 4
Measured ultimate strengths and failure modes

Specimen code	Section code	P_u (kN) / kN	Failure mode mode	Specimen code	Section code	P_u (kN) / kN	Failure mode mode
PP-1	C60×35×10×1.8	65.86	D+G	PP-12	C80×70×14×1.5	66.23	D+G
PP-2	C60×40×12×1.8	66.34	D+G	PP-13	C80×65×12×1.5	54.61	D+G
PP-3	C60×40×10×1.5	44.70	D+G	PP-14	C85×60×12×1.8	69.61	D+G
PP-4	C65×45×12×1.8	72.68	D+G	PP-15	C85×70×12×1.8	73.47	D+G
PP-5	C65×60×12×1.5	42.65	D+G	PP-16	C85×70×15×1.8	75.54	D+G
PP-6	C70×55×15×1.8	84.48	D+G	PP-17	C85×65×12×1.8	62.84	D+G
PP-7	C70×55×10×1.5	49.00	D+G	PP-18-1	C88×60×12×1.8	71.24	D+G
PP-8	C75×60×14×1.8	89.24	D+G	PP-18-2	C88×60×12×1.8	78.19	D+G
PP-9	C75×60×12×1.8	74.22	D+G	PP-19-1	C96×68×12×1.8	72.65	D+G
PP-10	C75×50×12×1.8	79.65	D+G	PP-19-2	C96×68×12×1.8	75.61	D+G
PP-11	C80×55×12×1.8	71.95	D+G				

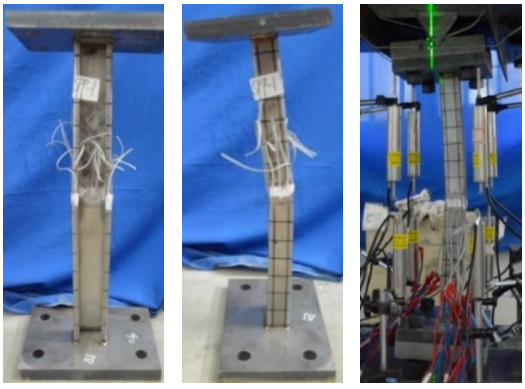

Fig. 20 Failure mode of PP-1

The failure modes of the above three types of specimens have the following common points: (1) after the test is loaded, no significant deformation was observed in all specimens in the early stage; (2) the overall buckling occurs before the distortional buckling; and (3) all the failure modes of the specimens show a certain degree of brittle failure, that is, when the ultimate strength is reached, the specimens suddenly fail and the bearing capacity drops sharply.

Fig. 21 The second category of failure mode

The member failure modes can be divided into three categories. In the first category, the specimen is bent toward the opening direction of the section as a whole, and the specimen with such failure is PP-1, as shown in Fig. 20. PP-1 is mainly dominated by global buckling.

In the second category, the specimens are bent toward the closed direction of the cross-section as a whole. The distortional buckling is outwardly convex. The specimens with this type are PP-3, PP-5, PP-6, PP- 7, PP-8, PP-9, PP-11, PP-13, PP-14, PP-18-1, PP-19-1 and PP-19-2, as shown in Fig. 21.

In the third category, the specimen is bent as a whole towards the closed direction of the section, and the distortional buckling is inwardly concave. The specimens with this type are PP-2, PP-4, PP-10, PP-12, PP-15, PP-16, PP-17 and PP-18-2, as shown in Fig. 22.

Fig. 22 The third type of failure mode

5. Comparison with predictions for design strength

No DSM for stainless steel lipped channels failed by distortional-overall interaction buckling in current specifications. However, the DSM for distortional buckling has been described in the AS/NZS [39] for carbon steel, AISI [40] for stainless steel, as well as the formulation established by Becque and Rasmussen [11] for stainless steel. To calculate the design strength of the lipped channel column failed by distortional-overall interaction buckling, the DSM for distortional buckling uses the member load (P_{ne}) instead of the yield load (P_y) for the definition of the distortional buckling slenderness (λ_d).

The test results are compared with the AS/NZS [39], AISI [40], as well as formulation proposed by Becque and Rasmussen's predictions [11], as shown in Fig. 23. DSM (AISI), DSM (AS/NZS) and DSM (Becque) in the figure indicate the results of bearing capacity calculations according to AISI, AS/NZS and Becque and Rasmussen calculation methods [11], respectively.

Most test data points are distributed under the DSM (AISI) curve and above the DSM (Becque) curve. The DSM (AS/NZS) curve does not have the same changing trend as the test results. DSM in AISI and AS/NZS for calculating the strength of the channels failing by distortional-overall interaction buckling was seen to be unconservative. DSM (Becque) curve is much closer to the test points than DSM in AISI and AS/NZS.

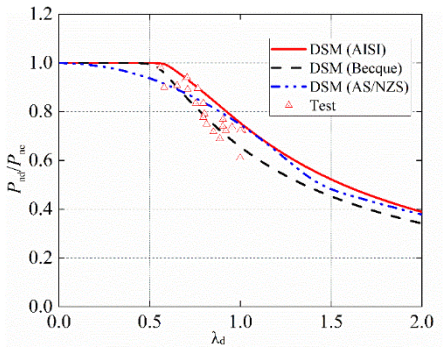

Fig. 21 The second type of failure mode

6. Conclusions

Axial compression tests on 21 columns were conducted to investigate the buckling damage characteristics of stainless steel columns. The focus of this experimental program is to study the distortional-overall interaction buckling. A 3-D laser scanner was used to measure the geometric imperfections. Material tensile tests were conducted to investigate the mechanical properties of stainless steel. Based on an analysis of the test results, the following general conclusions are made.

(1) All the test stainless steel lipped channel columns were successful in achieving interaction of distortional and global buckling about the minor axis.

(2) The member failure modes can be divided into three categories: 1) In the first category, the column is bent toward the opening direction of the section as a whole; 2) In the second category, the column is bent towards the closed direction of the cross section as a whole, and the distortional buckling is outwardly convex; 3) The third failure mode, the specimen is bent as a whole towards the closed direction of the section, and the distortional buckling is inwardly concave.

(3) The trends of the load-axial displacement relationships are the same. When the load is loaded, the axial displacements increase linearly with the load increases. As the load increases, the specimens' stiffness begin to decreases, and the load and displacement shows a nonlinear relationship until the stiffness decreases to zero. The nonlinear part of the curve are relatively short, and the load soon reaches the limit point.

(4) Both upper and lower support rotations are consistent, indicating that the stainless steel lipped channel cross sections were not twisted.

(5) Readings of both LVDT 2 and 4 are consistent, which indicates that the stainless steel lipped channel cross sections were not twisted. This is consistent with the conclusion identified in the load vs. rotation curves. The lateral displacements of both LVDT 2 and 4 are earlier and larger than the lateral displacements of both LVDT 1 and 5, which indicates that global buckling appears earlier than distortional buckling.

(6) DSM in AISI and AS/NZS for calculating the strength of stainless steel channels failing in distortional-overall interaction buckling are unconservative. The formulation proposed by Becque and Rasmussen is much closer to the test point than DSM in AISI and AS/NZS.

Acknowledgment

The authors would like to thank the financial support of the National Research Project Cultivation Fund of Southeast University Chengxian College (51878146) and National Natural Science Foundation of China (No. 52278153).

References

[1] Baddoo NR. Stainless steel in construction: A review of research, applications, challenges and opportunities. J. Constr. Steel Res. 2008; 64(11): 1199–1206.
[2] Gardner L. Stability and design of stainless steel structures – Review and outlook. Thin-Walled Struct. 2019; 141: 208–216.
[3] Sun Y., Su A., Jiang K., Liang Y. and Zhao O. Testing, numerical modelling and design of stainless steel welded I-sections under minor-axis combined loading. Engineering Structures, 2021, 243, 112513.
[4] Arrayago I, Real E, Gardner L. Description of stress–strain curves for stainless steel alloys [J]. Materials & Design, 2015(87): 540-552.
[5] Rasmussen K J R. Full-range stress–strain curves for stainless steel alloys [J]. Journal of Constructional Steel Research, 2003, 59(1): 47-61.
[6] Gardner L, Nethercot D A. Experiments on stainless steel hollow sections—Part 1: material and cross-sectional behaviour [J]. Journal of Constructional Steel Research, 2004, 60(9): 1291-1318.
[7] Tao Z, Rasmussen K J R. Stress-strain model for ferritic stainless steels [J]. Journal of Materials in Civil Engineering, 2016, 28(2): 1-5.
[8] Becque J, Rasmussen K J R. Experimental investigation of local-overall interaction buckling of stainless steel lipped channel columns [J]. Journal of Constructional Steel Research, 2009 (65): 1677-1684.
[9] Lecce M, Rasmussen K J R. Distortional buckling of cold-formed stainless steel sections: experimental investigation [J]. Journal of Structural Engineering, 2006, 132(4): 497-504.
[10] Kuwamura H. Local buckling of thin-walled stainless steel members [J]. Steel Structures, 2003(3): 191-201.
[11] Becque J, Lecce M, Rasmussen K J R. The direct strength method for stainless steel compression members [J]. Journal of Constructional Steel Research, 2008, 64(11): 1231-1238.
[12] Chen M , Fan S , Tao Y , et al. Design of the distortional buckling capacity of stainless steel lipped C-section columns[J]. Journal of Constructional Steel Research, 2018, 147(8.):116-131.
[13] Dobri J , Rossi B . Column Curves for Stainless Steel Lipped–Channel Sections[J]. Journal of Structural Engineering, 2020, 146(10):04020221.
[14] Fan S , Fang L , Zheng B , et al. Experimental study on bearing capacity of stainless steel lipped C section stub columns[J]. Thin-Walled Structures, 2014, 83(oct.):70-84.
[15] Barbara Rossi1; Jean-Pierre Jaspart; Kim J. R. Rasmussen. Combined Distortional and Overall Flexural-Torsional Buckling of Cold-Formed Stainless Steel Sections: Experimental Investigations[J]. Journal of Structural Engineering, 2010, 136(4): 354-360.
[16] Barbara Rossi1; Jean-Pierre Jaspart; Kim J. R. Rasmussen. Combined Distortional and Overall Flexural-Torsional Buckling of Cold-Formed Stainless Steel Sections: Design [J]. Journal of Structural Engineering, 2010, 136(4): 361-369.
[17] Chen M , Fan S , Li C , et al. Direct Strength Method for Stainless Steel Lipped Channel Columns Undergoing Local Buckling[J]. International Journal of Steel Structures, 2020:1-9.
[18] Lecce M, Rasmussen K J R. Distortional buckling of cold-formed stainless steel sections: Finite-element modeling and design [J]. Journal of Structural Engineering, 2006, 132(4): 505-514.
[19] Becque J, Rasmussen K J R. A numerical investigation of local–overall interaction buckling of stainless steel lipped channel columns [J]. Journal of Constructional Steel Research, 2009, 65(8): 1685-1693.
[20] Li S, Zhang L, Liang Y, and Zhao O. Experimental and numerical investigations of hot-rolled stainless steel channel section columns susceptible to flexural buckling [J]. Thin-Walled Struct. 164 (2021) 107791.
[21] S. Li, L. Zhang, O. Zhao, Global buckling and design of hot-rolled stainless steel channel section beam–columns [J]. Thin-Walled Struct. 170 (2022) 108433.
[22] S. Li, L. Zhang, O. Zhao, Testing, modelling and design of hot-rolled stainless steel channel sections under combined compression and minor-axis bending moment [J]. Thin-Walled Struct. 172 (2022) 108836.
[23 Liang Y, Zhao O, Long Y, et al. Experimental and numerical studies of laser-welded stainless steel channel sections under combined compression and major axis bending moment [J]. Thin-Walled Structures,2020, 157: 107035.
[24] Gardner L, Bu Y, Theofanous M. Laser-welded stainless steel I-sections: Residual stress measurements and column buckling tests - ScienceDirect[J]. Engineering Structures, 2016, 127(Nov.15):536-548.
[25] Yang L, Zhao M, Chan T M, et al. Flexural buckling of welded austenitic and duplex stainless steel I-section columns [J]. Journal of Constructional Steel Research, 2016, 122: 339-353.
[26] Becque J, Rasmussen K J R. Experimental investigation of the interaction of local and overall buckling of stainless steel I-columns [J]. Journal of Constructional Steel Research, 2009, 135(11): 1340-1348.
[27] Khate K, Patton M L, Marthong C. Structural behaviour of stainless steel stub column under axial compression: a FE study [J]. International Journal of Steel Structures, 2018, 18(5): 1723-40.
[28] Bredenkamp P J, Van Den Berg G J. The strength of stainless steel built-up I-section columns [J]. Journal of Constructional Steel Research, 1995 (34): 131-144.
[29] Anwar-Us-Saadat M, The continuous strength method for lateral-torsional buckling of stainless steel I-beams Ashraf M. [J]. Thin-Walled Structures, 2018(130): 148-60.
[30] Arrayago I , Real E . Experimental Study on Ferritic Stainless Steel RHS and SHS Cross-sectional Resistance Under Combined Loading[J]. Structures, 2015, 4:69-79.
[31] Liu Y, Young B. Buckling of stainless steel square hollow section compression members [J]. Journal of Constructional Steel Research, 2003, 59(2): 165-77.
[32] Theofanous M, Gardner L. Testing and numerical modelling of lean duplex stainless steel hollow section columns [J]. Engineering Structures, 2009, 31(12): 3047-58.
[33] Young B, Hartono W. Compression tests of stainless steel tubular members [J]. Journal of Structural Engineering, 2002, 128(6): 754-61.
[34] Young B, Liu Y. Experimental investigation of cold-formed stainless steel columns [J]. Journal of Structural Engineering, 2003, 129(2): 169-76.
[35] Rasmussen K J R, Hancock G J. Design of cold-formed stainless steel tubular members. I: columns [J]. Journal of Structural Engineering, 1993, 119(8): 2349-2367.
[36] National Standard of the People's Republic of China. Metallic materials-Tensile testing at ambient temperature [S]. Beijing: China Planning Press. 2010.
[37] B. Schafer. CUFSM software Version 5.0. Department of Civil Engineering, Johns Hopkins University, USA. (http://www.ce.jhu.edu/bschafer/cufsm/).
[38] National Standard of the People's Republic of China. Code for Acceptance of Construction Quality of Steel Structures (GB50205-2001) [S]. Beijing: China Planning Press. 2001.
[39] AS/NZS. Cold-formed stainless steel structures [S]. Australian/New Zealand-Standard, AS/NZS 4673:2001, Standards Australia, Sydney, Australia, 2001.
[40] North American Cold-Formed Steel Specification for the Design of Cold-Formed Steel structural Members [S]. American Iron and Steel Institute (AISI), Washington DC: 2016.